Shear-induced contact area anisotropy explained by a fracture mechanics model

A. Papangelo,[1,2] J. Scheibert,[3] R. Sahli,[3] G. Pallares,[3,4] and M. Ciavarella[1,2,*]

[1]*Dipartimento di eccellenza di Meccanica, Matematica e Management, Politecnico di Bari, Viale Japigia 182, 70126 Bari, Italy*

[2]*Department of Mechanical Engineering, Hamburg University of Technology, Am Schwarzenberg-Campus 1, 21073 Hamburg, Germany*

[3]*Univ Lyon, Ecole Centrale de Lyon, ENISE, ENTPE, CNRS, Laboratoire de Tribologie et Dynamique des Systèmes LTDS, UMR 5513, F-69134, Ecully, France*

[4]*CESI, LINEACT, Zone Aéroportuaire Méditerranée, 34130 Mauguio, France*

(Received 6 March 2019; published 30 May 2019)

This paper gives a theoretical analysis for the fundamental problem of anisotropy induced by shear forces on an adhesive contact, discussing the experimental data of the companion Letter. We present a fracture mechanics model where two phenomenological mode-mixity functions are introduced to describe the weak coupling between modes I and II or I and III, which changes the effective toughness of the interface. The mode-mixity functions have been interpolated using the data of a single experiment and then used to predict the behavior of the whole set of experimental observations. The model extends an idea by Johnson and Greenwood, to solve purely mode I problems of adhesion in the presence of a nonaxisymmetric Hertzian geometry, to the case of elliptical contacts sheared along their major or minor axis. Equality between the stress intensity factors and their critical values is imposed solely at the major and minor axes. We successfully validate our model against experimental data. The model predicts that the punch geometry will affect both the shape and the overall decay of the sheared contact area.

DOI: 10.1103/PhysRevE.99.053005

I. INTRODUCTION

The interplay of adhesion and friction is a problem of fundamental importance in tribology, which ideally should be solved at all scales from tectonic plates to atomic scales (for a recent review of multiscale methods and problems in tribology, see Ref. [1]). In the particular case of soft materials, it is already relatively well understood and plays a substantial role in Nature: in many insects, for example, an equivalent of an "adhesive Coulomb friction law" has been described, whereby the normal force to detach the adhesive "pads" is proportional to the shear force simultaneously applied [2–4]. For soft materials, a finite contact area is observed also under zero force due to adhesion [5] and as a consequence, friction is measured also under vanishing or even negative normal forces [6,7]. There is no unique framework to study this interaction [8]: for instance for hard materials, although no macroscopic adhesion is found and friction may have a number of origins, Rabinowicz [9,10] attempted to describe friction in terms of surface energy. Another example is the onset of sliding, for which fracture-like surface energy concepts have been used successfully [11–13].

Here we consider typically soft materials, for which the first fracture mechanics model and experiment for adhesion and friction interaction were conceived for macroscopic smooth spheres by Savkoor and Briggs [14], who extended the Johnson-Kendall-Roberts (JKR) model [5] to the presence of tangential force. This model, however, corresponded to a "purely brittle" model where the frictional resistance was neglected and, as such, *greatly underestimated* the interfacial toughness. In that respect, it has been observed that when mode I combines with mode II and/or mode III [see Fig. 1(a)], the interfacial toughness is greatly increased. The physical explanations for this increase are various (e.g., friction, plasticity, dislocation emission) and cannot be ascribed to a single phenomenon [16]. Since then a few phenomenological models have been proposed [17–23], which require a mode-mixity function (MMF) $f(\psi)$ [24] to describe the critical condition for propagation

$$G_c = G_{Ic} f(\psi), \tag{1}$$

where G_{Ic} is mode I critical factor (or surface energy, if we assume Griffith's concept), G_c is the critical energy release rate in mixed mode conditions, and ψ is the "phase angle":

$$\psi_2 = \arctan\left(\frac{K_{II}}{K_I}\right), \tag{2}$$

$$\psi_3 = \arctan\left(\frac{K_{III}}{K_I}\right), \tag{3}$$

where K_{III}, K_{II}, and K_I, respectively, are the mode III, mode II, and mode I stress intensity factors.

The most recent model in this field is perhaps that by Papangelo and Ciavarella [23] who compared it with recent experimental measurements by Mergel *et al.* [8] and concluded that the transition to sliding is very sensitive to the choice of the MMF. Papangelo and Ciavarella's mode-mixity model [23] suggests that upon shearing the contact can experience either a smooth transition from the JKR to the Hertzian contact area or an unstable jump to the Hertzian solution where lighter normal forces favor the latter behavior. All linear elastic fracture mechanics (LEFM) models indicate a decay of the

*mciava@poliba.it

contact area with force, but the overall evolution strongly depends on the effective form of the MMF [23]. Furthermore, the most up-to-date experimental evidence shows that for high normal forces, the decay of the contact area with the tangential force is quadratic [15], while for small normal forces [8] it isn't. Experimental measurements of contact area evolution show that the shape of the contact area is circular, according to JKR theory, at zero tangential force and shrinks in an elliptical-like fashion while the shear force is increased ([8,15,19]). So far all LEFM models proposed [14,17–19,22,23] make the approximation to consider the contact as circular, even when sheared. This requires an averaging of the effects of mode II and mode III around the periphery. However, it is well known that sphere-plane contacts lose their initial circularity when submitted to shear, indicating that axisymmetry is a very questionable assumption. Note that recent experimental investigations for rough interfaces composed of many asperities [15] have showed similar anisotropic real area reduction and morphology changes, as discussed extensively in the companion Letter [25]. A better understanding of the simpler sphere-plane contacts is crucial to comprehend shear-induced anisotropy in rough contacts.

In the present paper, we shall extend the axisymmetric theory to include the case of elliptical shrinking of a single contact area with the shear force, starting from either a circular or even already elliptical contact area. Initial ellipticity typically occurs in the case of rough contacts, where most summits are mildly elliptical, the most common ratio of principal summit curvatures being near 2:1 [26].

The only assumption we make for simplicity is that either the major or the minor axis of the contact ellipse is aligned with the shear force: results will show a sufficiently clear overall picture. In the first part of the paper the theoretical model will be introduced, while in the second part it will be validated against the experimental results provided in the companion Letter [25] and in Sahli *et al.* [15].

II. THE APPROXIMATE JKR THEORY FOR ELLIPTICAL CONTACTS

In absence of tangential force, Johnson and Greenwood [27] (JG in the following) developed an approximate JKR theory for adhesion of an Hertzian profile with differing principal radii of curvature. The contact problem is solved "approximately" in a sense that the equality of the stress intensity factor (SIF) to its critical value K_{Ic} around the periphery is satisfied only at the major and minor axis of the contact ellipse. JG assume a pressure distribution equal to

$$p(x,y) = \frac{p_1 - \alpha x^2 - \beta y^2}{\sqrt{1-(x/a)^2-(y/b)^2}}, \tag{4}$$

where a and b are, respectively, the major and minor semiaxes of the ellipse, (p_1, α, β) are constants to be found, and $p(x,y)$ is taken positive (negative) when compressive (tensile). The stress intensity factors at the major and minor axis (respectively, a and b) are

$$K_I(a) = (\alpha a^2 - p_1)\sqrt{\pi a} = K_{Ic}, \tag{5}$$

$$K_I(b) = (\beta b^2 - p_1)\sqrt{\pi b} = K_{Ic}. \tag{6}$$

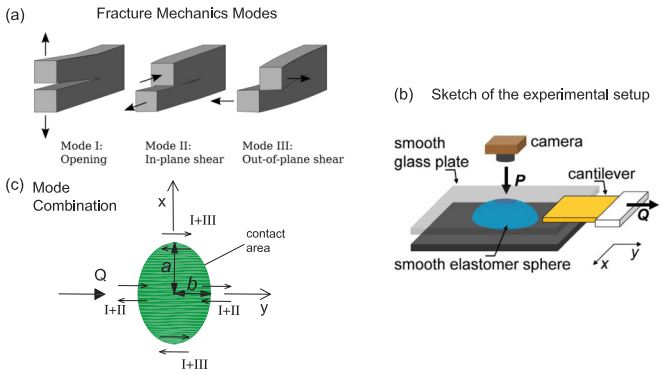

FIG. 1. (a) Fracture mechanics rupture modes (from Ref. [30]). (b) Sketch of the experimental setup used in Ref. [15], and in the companion Letter [25]. (c) Combination of the modes along the periphery of the contact patch.

JG impose the SIF at the major and minor axis to be equal to its critical value which, by standard LEFM arguments, is $K_{Ic} = \sqrt{2E^* G_{Ic}}$, where E^* is the plane strain composite modulus of the interface, and G_{Ic} the mode I "toughness" or surface energy. Galin's [28] theorem establishes that any pressure distribution of the form (4) produces a field of quadratic displacements

$$w = w_{00} - w_{20}x^2 - w_{02}y^2, \tag{7}$$

where w_{00} is the indentation and (w_{20}, w_{02}) are constants to be found. Kalker [29] reveals the relation between the sets of constants (α, β) and (w_{20}, w_{02}):

$$\begin{bmatrix} w_{20} \\ w_{02} \end{bmatrix} = \left(\frac{b}{E^*}\right)\begin{bmatrix} (\boldsymbol{D}+\boldsymbol{C})\alpha - (b/a)^2\boldsymbol{C}\beta \\ -\boldsymbol{C}\alpha + \{\boldsymbol{B} + (b/a)^2\boldsymbol{C}\}\beta \end{bmatrix} = \begin{bmatrix} 1/2R_1 \\ 1/2R_2 \end{bmatrix}, \tag{8}$$

where $\boldsymbol{K}(e), \boldsymbol{E}(e), \boldsymbol{B}(e), \boldsymbol{C}(e), \boldsymbol{D}(e)$ are complete elliptic integrals of argument $e = \sqrt{1-g^2}$ $(g = b/a < 1)$ with $e^2\boldsymbol{D}(e) = \boldsymbol{K}(e) - \boldsymbol{E}(e)$, $\boldsymbol{B}(e) = \boldsymbol{K}(e) - \boldsymbol{D}(e)$, $e^2\boldsymbol{C}(e) = \boldsymbol{D}(e) - \boldsymbol{B}(e)$, and (R_1, R_2) are the principal radii of curvature. The problem is closed adding the equation for the total normal force P:

$$P = 2\pi ab\left[p_1 - \frac{1}{3}(\alpha a^2 + \beta b^2)\right] \tag{9}$$

or for the indentation $\delta\ (= w_{00})$ [29]

$$\delta = \left(\frac{b}{E^*}\right)[2p_1\boldsymbol{K} - \alpha a^2\boldsymbol{B} - \beta b^2\boldsymbol{D}], \tag{10}$$

which, in the original case of JG, closes the system of five equations [(5), (6), (8), (9)—or (10)] in the five unknowns $(a, b, p_1, \alpha, \beta)$. For $R_1 = R_2$ this corresponds to the classical JKR solution.

III. THE EFFECT OF TANGENTIAL FORCE

A. Theoretical model

Assume that we have a sphere of radius R in adhesive contact with a half space [see Fig. 1(b)].

If a tangential shearing force Q is applied, and no slip occurs in the contact area, a singular shear traction distribution of the form

$$q(x,y) = q_0/\sqrt{1-(x/a)^2-(y/b)^2} \tag{11}$$

will arise at the interface. Experimental inspection of contact area in this condition shows the contact patch is nearly elliptical and shrinks along the direction of the applied shearing force (mode II), while remaining slightly affected in the perpendicular direction (mode III) [see sketch in Fig. 1(c), the companion Letter [25], and Refs. [8,15,19]]. A shear traction distribution of the form (11) gives a tangential force $Q = 2\pi abq_0$ and produces at the major axis $K_{II}(a) = 0$ and $K_{III}(a) = q_0\sqrt{\pi a}$, while at the minor axis, $K_{II}(b) = q_0\sqrt{\pi b}$, $K_{III}(b) = 0$. The energy release rate according to standard fracture mechanics arguments is $G = \frac{1}{2E^*}(K_I^2 + K_{II}^2 + \frac{1}{1-\nu}K_{III}^2)$; thus using (5) and (6) the equivalent SIF at the major "a" and minor "b" axes is

$$K_{\rm eq}(a) = \sqrt{K_I^2(a) + \frac{1}{1-\nu}K_{III}^2(a)} = \sqrt{(\alpha a^2 - p_1)^2 + 2q_0^2}\sqrt{\pi a}, \tag{12}$$

$$K_{\rm eq}(b) = \sqrt{K_I^2(b) + K_{II}^2(b)} = \sqrt{(\beta b^2 - p_1)^2 + q_0^2}\sqrt{\pi b}. \tag{13}$$

The critical energy needed for the external crack to advance, G_c, depends on the "mode mixity." Following Hutchinson and Suo [24] we shall postulate that G_c depends on the phase angles $\psi_2 = \arctan(\frac{K_{II}}{K_I})$ and $\psi_3 = \arctan(\frac{K_{III}}{K_I})$; thus at the minor (where we have modes I and II) and major (where we have modes I and III) axes we write, respectively, $G_c = G_{Ic}f_{II}(\psi_2)$ and $G_c = G_{Ic}f_{III}(\psi_3)$:

$$\sqrt{(\beta b^2 - p_1)^2 + q_0^2}\sqrt{\pi b} = K_{Ic}\sqrt{f_{II}(\psi_2)}, \tag{14}$$

$$\sqrt{(\alpha a^2 - p_1)^2 + \frac{1}{1-\nu}q_0^2}\sqrt{\pi a} = K_{Ic}\sqrt{f_{III}(\psi_3)}, \tag{15}$$

where $f_{II}(\psi_2)$ and $f_{III}(\psi_3)$ are two MMFs which take into account the mixed-mode dependent toughness of the interface.

To sum up, the problem is reduced to a system of five equations in the five unknown $(a, b, p_1, \alpha, \beta)$:[1]

$$\begin{aligned}
&\sqrt{(\beta b^2 - p_1)^2 + q_0^2}\sqrt{\pi b} - \sqrt{2E^*G_{Ic}f_{II}(\psi_2)} = 0\\
&\sqrt{(\alpha a^2 - p_1)^2 + \frac{1}{1-\nu}q_0^2}\sqrt{\pi a} - \sqrt{2E^*G_{Ic}f_{III}(\psi_3)} = 0,\\
&\left(\frac{b}{E^*}\right)[(\boldsymbol{D} + \boldsymbol{C})\alpha - (b/a)^2\boldsymbol{C}\beta] - \frac{1}{2R_1} = 0\\
&\left(\frac{b}{E^*}\right)[-\boldsymbol{C}\alpha + \{\boldsymbol{B} + (b/a)^2\boldsymbol{C}\}\beta] - \frac{1}{2R_2} = 0\\
&P - 2\pi ab\left[p_1 - \frac{1}{3}(\alpha a^2 + \beta b^2)\right] = 0
\end{aligned} \tag{16}$$

where, if the punch is axisymmetric[2] $R_1 = R_2 = R$. In principle, if one knows how the interfacial toughness depends on the mode combination, this problem can be solved exactly, with the sole approximation that the equality of the SIFs with their critical values is guaranteed only at the major and minor axes in line with the JG approximation.

Next, the following dimensionless notation is introduced [31]:

$$\begin{aligned}
&\gamma = \sqrt{\frac{R_2}{R_1}}, \quad R_e = \sqrt{R_2R_1}, \quad \xi = \left(\frac{E^*R_e}{G_{Ic}}\right)^{1/3},\\
&\widetilde{a} = \frac{\xi a}{R_e}, \quad \widetilde{b} = \frac{\xi b}{R_e}, \quad g = \frac{b}{a}, \quad \widetilde{\delta} = \frac{\xi^2\delta}{R_e},\\
&\widetilde{Q} = \frac{Q}{R_eG_{Ic}}, \quad \widetilde{P} = \frac{P}{R_eG_{Ic}}, \quad \widetilde{\alpha} = \frac{R_e^2\alpha}{\xi E^*},\\
&\widetilde{\beta} = \frac{R_e^2\beta}{\xi E^*}, \quad \widetilde{p}_1 = \frac{\xi p_1}{E^*}, \quad \widetilde{q}_0 = \frac{\xi q_0}{E^*},
\end{aligned} \tag{17}$$

and the system of Eq. (16) is written in dimensionless form:

$$\begin{aligned}
&\sqrt{(\widetilde{\beta}g^2\widetilde{a}^2 - \widetilde{p}_1)^2 + \left(\frac{\widetilde{Q}}{2\pi\widetilde{a}^2g}\right)^2}\sqrt{\pi g\widetilde{a}} - \sqrt{2f_{II}(\psi_2)} = 0\\
&\sqrt{(\widetilde{\alpha}\widetilde{a}^2 - \widetilde{p}_1)^2 + \frac{1}{1-\nu}\left(\frac{\widetilde{Q}}{2\pi\widetilde{a}^2g}\right)^2}\sqrt{\pi\widetilde{a}} - \sqrt{2f_{III}(\psi_3)} = 0,\\
&\widetilde{a}g[(\boldsymbol{D} + \boldsymbol{C})\widetilde{\alpha} - g^2\boldsymbol{C}\widetilde{\beta}] - \frac{\gamma}{2} = 0\\
&\widetilde{a}g[-\boldsymbol{C}\widetilde{\alpha} + \{\boldsymbol{B} + g^2\boldsymbol{C}\}\widetilde{\beta}] - \frac{1}{2\gamma} = 0\\
&\widetilde{P} - 2\pi g\widetilde{a}^2\left[\widetilde{p}_1 - \frac{\widetilde{a}^2}{3}(\widetilde{\alpha} + \widetilde{\beta}g^2)\right] = 0
\end{aligned} \tag{18}$$

where we used $\widetilde{q}_0 = \frac{\widetilde{Q}}{2\pi\widetilde{a}^2g}$. If, in place of the normal force $\widetilde{P}$, the normal indentation $\widetilde{\delta}$ is controlled, the last equation in (18) is replaced by

$$\widetilde{\delta} = \widetilde{b}[2\widetilde{p}_1\boldsymbol{K} - \widetilde{\alpha}\widetilde{a}^2\boldsymbol{B} - \widetilde{\beta}\widetilde{b}^2\boldsymbol{D}]. \tag{19}$$

For a tangential displacement controlled experiment we recall that an elliptical shear distribution as in (11) produces a uniform tangential displacement δ_T equal to [32]:

$$\delta_T = \frac{Q}{\pi aE^*(1-\nu)}\left[\boldsymbol{K} - \frac{\nu}{1-g^2}(\boldsymbol{K} - \boldsymbol{E})\right]; \quad b < a, \tag{20}$$

where we used the identity $E^* = \frac{E}{1-\nu^2}$ and $q_0 = \frac{Q}{2\pi ab}$. In dimensionless form $\widetilde{\delta}_T = \delta_T\xi^2/R$ gives

$$\widetilde{\delta}_T = \frac{\widetilde{Q}}{\pi\widetilde{a}(1-\nu)}\left[\boldsymbol{K} - \frac{\nu}{1-g^2}(\boldsymbol{K} - \boldsymbol{E})\right]; \quad \widetilde{b} < \widetilde{a}, \tag{21}$$

so that $\widetilde{Q}$ may be replaced by $\widetilde{\delta}_T$ in (18).

Although the theoretical model has been derived with the hypothesis of having the tangential force Q aligned with the minor axis [the y direction in Figs. 1(b) and 1(c)], it can be trivially rewritten with Q aligned with the major axis.

[1]The last equation for the force can be replaced by the respective for indentation (10).

[2]In deriving the model we start with the case of a sheared spherical punch. Nevertheless the model can be also used for non-axisymmetric Hertzian geometry provided that the tangential force is aligned with the minor or major axis.

B. MMF estimation

As shown in Ref. [23] for the axisymmetric case, the model results are very sensitive to the exact choice of the phenomenological MMF. After testing the Literature models available, e.g., the models proposed by Ref. [24], we decided to extract the MMF from a calibration experiment.

Assume that for a given experimental setup we know the geometry (R_1, R_2), the applied normal force P (or indentation δ), and for each tangential force Q the corresponding semiaxes of the contact patch (a, b). It is possible to estimate the MMFs $f_{II}(\psi_2)$ and $f_{III}(\psi_3)$ by the following procedure. First, from the third and fourth equations of Eqs. (18) one obtains $(\widetilde{\alpha}, \widetilde{\beta})$

$$\widetilde{\alpha} = \frac{\gamma^2 \boldsymbol{B} + (1+\gamma^2) g^2 \boldsymbol{C}}{2\widetilde{a} g \gamma [g^2 \boldsymbol{C}\boldsymbol{D} + \boldsymbol{B}(\boldsymbol{C}+\boldsymbol{D})]}, \tag{22}$$

$$\widetilde{\beta} = \frac{(1+\gamma^2)\boldsymbol{C} + \boldsymbol{D}}{2\widetilde{a} g \gamma [g^2 \boldsymbol{C}\boldsymbol{D} + \boldsymbol{B}(\boldsymbol{C}+\boldsymbol{D})]}, \tag{23}$$

then, using the fifth equation of Eqs. (18) one computes $\widetilde{p}_1$:

$$\widetilde{p}_1 = \frac{\widetilde{P}}{2\pi g \widetilde{a}^2} + \frac{\widetilde{a}^2}{3}(\widetilde{\alpha} + \widetilde{\beta} g^2), \tag{24}$$

and finally from the first and second equations of Eqs. (18) one obtains

$$f_{II,\mathrm{exp}}(\psi_2) = \frac{\pi g \widetilde{a}}{2}\left[(\widetilde{\beta} g^2 \widetilde{a}^2 - \widetilde{p}_1)^2 + \left(\frac{\widetilde{Q}}{2\pi \widetilde{a}^2 g}\right)^2\right], \tag{25}$$

$$f_{III,\mathrm{exp}}(\psi_3) = \frac{\pi \widetilde{a}}{2}\left[(\widetilde{\alpha}\widetilde{a}^2 - \widetilde{p}_1)^2 + \frac{1}{1-\nu}\left(\frac{\widetilde{Q}}{2\pi \widetilde{a}^2 g}\right)^2\right]. \tag{26}$$

The corresponding phase angles will be for mode I-II interaction

$$\psi_2 = \arctan\left(\frac{K_{II}}{K_I}\right) = \arctan\left[\frac{\widetilde{Q}}{2\pi \widetilde{a}^2 g(\widetilde{\beta}\widetilde{a}^2 g^2 - \widetilde{p}_1)}\right] \tag{27}$$

and for mode I-III interaction

$$\psi_3 = \arctan\left(\frac{K_{III}}{K_I}\right) = \arctan\left[\frac{\widetilde{Q}}{2\pi \widetilde{a}^2 g(\widetilde{\alpha}\widetilde{a}^2 - \widetilde{p}_1)}\right]. \tag{28}$$

IV. COMPARISON WITH EXPERIMENTAL RESULTS

A. Determining the MMF

Let us consider the experimental data discussed in the companion Letter [25] and in Ref. [15]. The experimental setup is composed of a cantilever which sustains a glass substrate which is pressed against a PDMS sphere of radius R and then sheared [see Fig. 1(c)]. A camera was used to track the contact area evolution while a force cell simultaneously measured the tangential force applied. The experimental results reported in Ref. [15] and further analyzed in the companion Letter [25] are provided for the following set of normal forces $P = [0.27, 0.55, 0.82, 1.10, 1.37, 1.65, 1.92, 2.12]$ N, which span one order of magnitude, and for the following sphere radius $R = 9.42$ mm.

To estimate the MMFs the aforementioned procedure was used—the equations (22), (23), (24), (25), and (26)—for the arbitrarily selected data corresponding to the case $P = 0.55$ N.[3] For the PDMS-glass interfaces we used the following material properties (see Ref. [15] and their Supporting Information):

$$G_{Ic} = 27\ \mathrm{mJ/m^2}, \quad E = 1.88\ \mathrm{MPa},$$
$$\nu = 0.5, \quad \sigma = 0.41\ \mathrm{MPa}, \tag{29}$$

where σ is the best fitted average shear strength of the interface (see Fig. 4 below) and E was obtained from the control experiment[4] with $P = 0.55$ N. Figure 2(a) shows the experimental data (orange triangles) and the

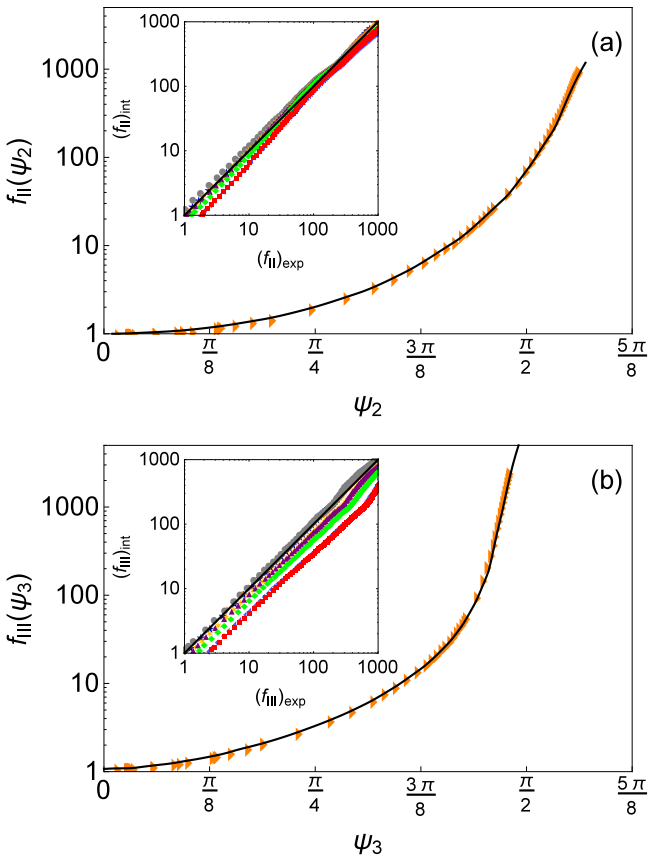

FIG. 2. Orange triangles: mode-mixity functions (a) $f_{II}(\psi_2)$ [respectively, (b) $f_{III}(\psi_3)$] estimated from Eq. (25) [respectively, (26)] from the experimental data of case $P = 0.55$ N. Solid lines: interpolation of the curves used in the comparison with other experimental data available in the companion Letter [25]. Insets: interpolated vs experimental MMFs for all experiments. Solid lines: equality lines. Markers for experimental results. Blue stars, orange right-triangles, gray circles, yellow stars, purple up-triangles, green diamonds, violet left-triangles, red squares, respectively, for $P = [0.27, 0.55, 0.82, 1.10, 1.37, 1.65, 1.92, 2.12]$ N.

[3]Similar results can be obtained selecting the set of data corresponding to a different normal force.

[4]For the control experiment with $P = 0.55$ N, under zero tangential force, a contact area $A_0 \simeq 4.48\ \mathrm{mm}^2$ was measured. Using the JKR relation $P = \frac{4E^*}{3R}\left(\frac{A_0}{\pi}\right)^{3/2} - \sqrt{8\pi^{-1/2}E^* {A_0}^{3/2} G_{Ic}}$ with $G_{Ic} = 27\ \mathrm{mJ/m^2}$, $\nu = 0.5$ and $R = 9.42$ mm one gets $E \simeq 1.88$ MPa.

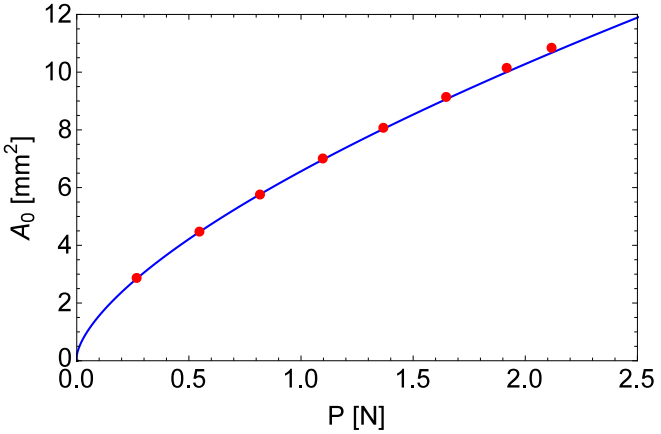

FIG. 3. Contact area under null tangential force A_0 vs normal force P. Solid line: JKR model with $G_{Ic} = 27$ mJ/m^2, $E = 1.88$ MPa, $\nu = 0.5$, and $R = 9.42$ mm. Red dots: experimental data under null tangential force.

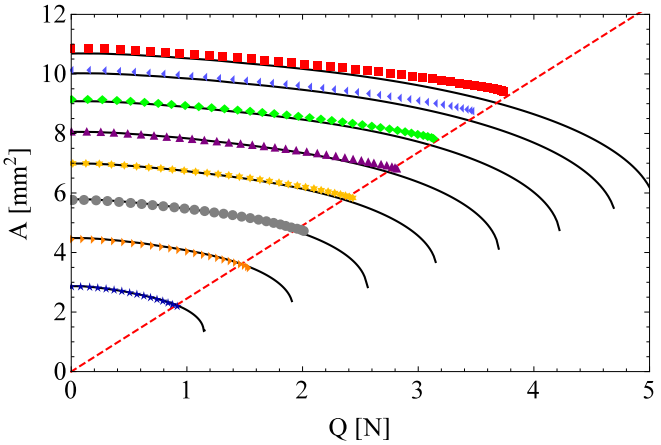

FIG. 4. Contact area A as a function of the tangential force Q for different normal forces $P = [0.27, 0.55, 0.82, 1.10, 1.37, 1.65, 1.92, 2.12]$ N and $R_e = R = 9.42$ mm. The markers indicate the experimental measurements, the solid black lines show the model prediction, and the dashed red line indicates the full sliding criterion $Q_s = \sigma A$ with $\sigma = 0.41$ MPa.

interpolated (black solid line) MMF $f_{II}(\psi_2)$ as a function of the phase angle ψ_2. $f_{II}(\psi_2)$ can be well approximated by $\log[f_{II}(\psi_2)] = a_2\psi_2^2 + b_2\psi_2^{n_2}$, where the coefficients are $(a_2, b_2, n_2) = (1.18, 5.67 \times 10^{-2}, 7.05)$. To obtain a better fit, the data were interpolated in log-linear form, $(\psi_2, \log[f_{II}(\psi_2)])$, which allows us to catch the MMF across all scales. The inset shows the interpolated mode-II MMF versus the one evaluated from all the set of experimental data available, which collapse over three orders of magnitude of f_{II}. With the same procedure, $f_{III}(\psi_3)$ has been interpolated from the experimental data using solely the set of data corresponding to the case $P = 0.55$ N [Fig. 2(b)]. $f_{III}(\psi_3)$ can be well approximated by $\log[f_{III}(\psi_3)] = a_3\psi_3^2 + b_3\psi_3^{n_3}$, where the coefficients are $(a_3, b_3, n_3) = (1.87, 6.73 \times 10^{-3}, 15.20)$. The inset shows that the complete set of experimental data align along the main diagonal, nevertheless the data referring to the higher normal forces, $P \approx [1.65, 1.92, 2.12]$ N, appear to be shifted by a factor ≈ 2 also for vanishing tangential forces $[f(\psi) \simeq 1]$, which indicates a small deviation in the original JKR fit (see the three rightmost points in Fig. 3). It is worth noting that the normal force is varying by one order of magnitude in the same set of experiments, hence some nonlinear effects (probably due to stiffening in the material) may have arisen which make the JKR fit not perfect. Figure 3 shows the JKR curve (black solid line) obtained with the parameters reported in the companion Letter [25] and in Ref. [15] [see (29)] and for each normal force the contact area under null shear force (red dots). It can be observed that the deviations from JKR are very small.

B. Decay of contact area

In this section the results obtained solving the system of equations (18) are presented, where the unknown MMFs $f_{II}(\psi_2)$ and $f_{III}(\psi_3)$ have been substituted by the one estimated in the previous section using only the data set for $P = 0.55$ N. Figure 4 shows the contact area evolution as a function of the tangential force for the complete set of experimental data from Ref. [15] with $R_e = R = 9.42$ mm (PDMS sphere-glass substrate contact). The markers indicate the experimental results obtained for each normal force, while the black solid lines are for the proposed model, which proves to be in very good agreement with all the observations. Small deviations appear for the heavier normal forces as was already found and discussed in the previous section. The dashed red line shows the full sliding threshold according to the criterion $Q_s = \sigma A$, as proposed in Refs. [15] and [8]. Figure 5 favorably compares the mean shear stress at the interface $\overline{\sigma} = Q/A$ according to the experimental results (markers) and to the proposed model (solid black lines), where the red dashed lines mark the boundary of the full sliding region, $\overline{\sigma} = \sigma = 0.41$ MPa.

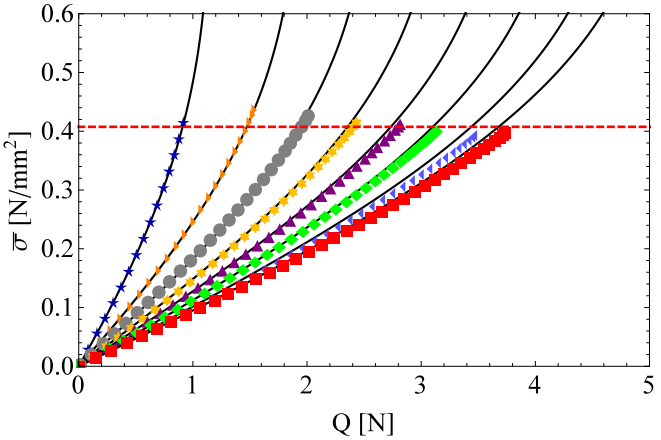

FIG. 5. Mean shear stress at the interface $\overline{\sigma} = Q/A$ according to the experimental results from Ref. [15] (markers) and to the proposed model (solid black lines). The solid lines are drawn for $P = [0.27, 0.55, 0.82, 1.10, 1.37, 1.65, 1.92, 2.12]$ N and $R_e = R = 9.42$ mm. The red dashed line marks the full sliding points at $\overline{\sigma} = \sigma = 0.41$ MPa.

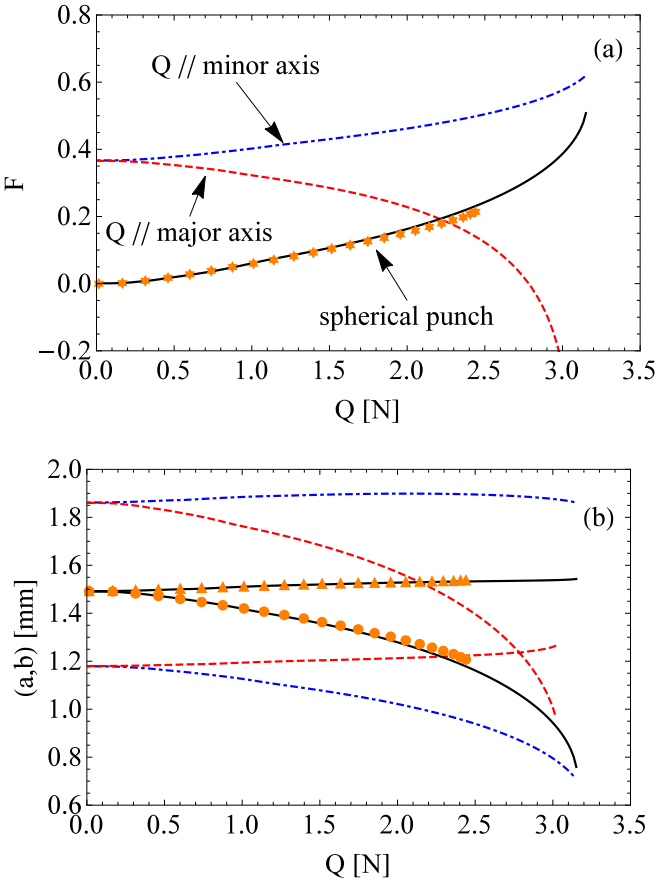

FIG. 6. (a) Ellipticity $F = 1 - b/a$ versus the tangential force Q as obtained experimentally for $P = 1.10$ N, $R_e = R = 9.42$ mm (orange stars) and as obtained from the model (solid black line). Prediction of the ellipticity evolution for a nonaxisymmetric punch with $R_2/R_1 = 1/2$ ($R_e = 9.42$ mm) loaded along its major (dashed red line) or minor (blue dot-dashed line) axis. (b) Evolution of the the semiaxes (a, b), with $a > b$ at $Q = 0$ N. Symbols and lines as in panel (a).

V. CONTACT SHEARING ALONG THE MAJOR-MINOR SEMIAXES

Let us compare the model predictions with the experimental results in terms of evolution of the ellipticity (or flattening) $F = 1 - b/a$. For this comparison, the set of experimental data for $P = 1.10$ N and $R_e = R = 9.42$ mm has been chosen. In Fig. 6(a) the ellipticity is plotted against the tangential force Q: the experimental data are plotted with orange stars, while the model prediction is shown as a black solid line. The same set of data is plotted in Fig. 6(b) in terms of evolution of the semiaxes (a, b). Notice that the contact area shrinks drastically along the direction aligned with the tangential force, semiaxis "b," while the perpendicular axis "a" remains mostly unaffected by the tangential force. This is in agreement with the observation that the interfacial toughness under the mode combination I-III was found greater than under mode I-II combination [compare $f_{II}(\psi_2)$ and $f_{III}(\psi_3)$ in Fig. 2]. The predictions are in excellent agreement with the experimental results of Ref. [25].

We then investigated the indentation of a nonaxisymmetric punch with $R_e = R = 9.42$ mm and $R_2/R_1 = 1/2$, as in the typical rough contacts according to Ref. [26], all the other parameters being unchanged. For the latter case no experimental data are available to compare with, thus only the model predictions are presented. Figure 6(a) shows the evolution of the ellipticity when the punch is loaded along its major (red dashed line) and minor (blue dotdashed line) axis. The same results are plotted in terms of semiaxes evolution in Fig. 6(b). Notice that after shearing, the contact patch shapes are strongly different among the three cases we have analyzed, i.e., axisymmetric punch and nonaxisymmetric punch loaded along the major or minor axis. Indeed, the axis under mode II loading tends to shrink much more rapidly with respect to the axis under mode III loading. Hence the punch loaded along its major axis shrinks towards a more circular shape, i.e., the ellipticity decreases and eventually becomes negative as due to the shearing force, we obtain $a < b$. On the other hand, loading along the minor axis produces a contact patch with increasing ellipticity while Q is increased.

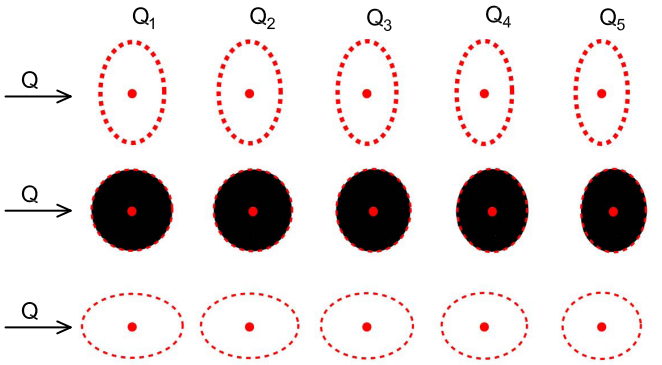

FIG. 7. Evolution of the contact patches according to the proposed model (red dashed line) for $R_2/R_1 = 1/2, R_e = R$ loaded, respectively, along the minor (top row) and major (bottom row) axis and for $R_1 = R_2 = R$ (middle row). For the axisymmetric case (middle row) experimental contact patches are plotted in black. The tangential forces range from Q_1 to Q_5, respectively [0.04, 0.77, 1.42, 1.98, 2.38] N. For all the snapshots $P = 1.10$ N.

The theoretical model is based on the assumption that the contact area shrinks in an elliptical fashion while the contact is sheared. In Fig. 7 we check this assumption comparing with actual experimental snapshots of the contact area (same data used for Fig. 6) taken for five tangential forces, from Q_1 to Q_5, respectively [0.04, 0.77, 1.42, 1.98, 2.38] N. The results are reported for $R_e = R$ and, respectively, $R_2/R_1 = 1$ (middle row) and $R_2/R_1 = 1/2$ (top and bottom row) where the shearing force is aligned with the minor (top row) and major (bottom row) axis. The evolution of the contact patches according to the proposed model is shown as a red dashed line (all rows), while the experimental contact patches are plotted as a black patch (middle row). The agreement between experimental results and model prediction is excellent for the axisymmetric punch, while we can provide only predictions for $R_2/R_1 = 1/2$ because experimental data are missing.

Finally, we further explore the effect of the initial geometry, R_2/R_1 ratio, on the contact area decay. In Fig. 8 the evolution of contact area with the tangential force is reported for $R_e = R = 9.42$ mm, $P = 1.10$ N,

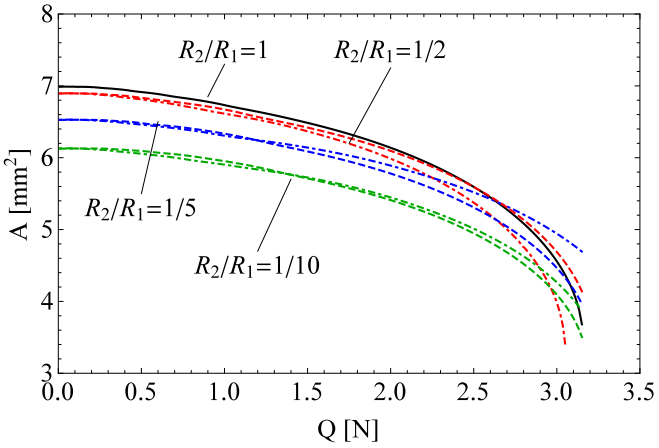

FIG. 8. Evolution of the contact area with the tangential force reported for $R_e = R = 9.42$ mm, $P = 1.10$ N, $R_2/R_1 = [1, 1/2, 1/5, 1/10]$, respectively, solid black line and red, blue, and green lines. Predictions have been made for both Q aligned with the major (dot-dashed lines) and minor (dashed lines) axis.

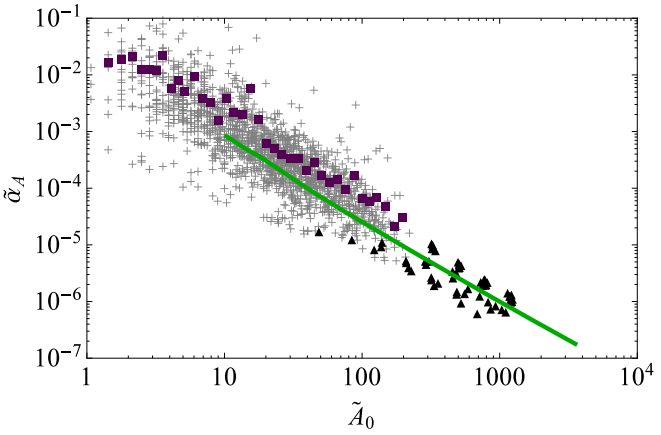

FIG. 9. Greeen solid line: coefficient $\widetilde{\alpha}_A$ obtained fitting the numerical data obtained by the proposed elliptical model with a power law function $\widetilde{A}(Q) = \widetilde{A}_0 - \widetilde{\alpha}_A \widetilde{Q}^2$ as proposed by Ref. [15] as a function of $\widetilde{A}_0$. Symbols represent the experimental data reported in Ref. [15]: triangles for smooth sphere with radii $R = [7.06, 9.42, 24.81]$ mm, crosses refer to the experimental data obtained for microjunctions (rough contact), and average values indicated by purple squares.

$R_2/R_1 = [1, 1/2, 1/5, 1/10]$, respectively, solid black line and red, blue, and green lines. Predictions have been made for both Q aligned with the major (dot-dashed lines) and minor (dashed lines) axis. One concludes that the contact shapes are affected by both the punch geometry and the direction of shear with respect to the ellipse orientation. Inspection of Fig. 8 reveals that in terms of overall contact area decay for increasing shear force Q, changing the ratio R_2/R_1 from 1 to 1/10 will produce a reduction of the overall contact area of the order of 10%–15% for both Q aligned along the major (dot-dashed line) or minor (dashed) axis.

VI. SCALING LAW FOR AREA DECAY

Reference [15] shows that for smooth spheres a quadratic form $A(Q) = A_0 - \alpha_A Q^2$ well captures the decay of contact area with tangential force, where A_0 is the contact area for $Q = 0$ N and α_A is a fitting coefficient. Interestingly, these authors found that α_A shows a power law scaling with A_0 with exponent $-3/2$ over four orders of magnitude, which comprises data from interfacial microjunctions (rough contacts) and data from smooth spheres. Literature LEFM axisymmetric models for smooth spheres [22,23] have found a similar but not equal exponent, $-5/4$.

Here we investigate which scaling law would arise from the present elliptical model and compare with experimental results. We defined a set of normal forces ranging from 1 mN to 10 N and, using the model, obtained the area versus tangential force curves up to full sliding, truncating them at $Q_s = \sigma A$. We used the same material properties (29) and geometry parameters $R_e = R = 9.42$ mm adopted in the previous analyses. The resulting curves were fitted with a quadratic area decay law that in dimensionless form reads $\widetilde{A}(\widetilde{Q}) = \widetilde{A}_0 - \widetilde{\alpha}_A \widetilde{Q}^2$, where $\widetilde{A} = A(\xi/R_e)^2$ and $\widetilde{\alpha}_A = \alpha_A(\xi G_{Ic})^2$. To this end we needed to estimate the mean microjunction radius. We consider the results of a single rough contact experiment from Ref. [15]: PDMS-glass contact, under a normal force of $P = 6.40$ N for which 514 microcontacts with an initial area larger than 2×10^{-9} m^2 were found and tracked. This results in an average force for each microjunction equal to $P_i = 6.4/514 \simeq 1.2 \times 10^{-2}$ N. From the distribution of microjunctions contact areas we derived the characteristic dimension of the microjunction $a_i = \sqrt{A_i/\pi}$ and computed the mean contact radius $\overline{a}_i = 0.235$ mm. Using the JKR model with known P_i, a_i and material properties $G_{Ic} = 27$ mJ/m^2, $E = 1.88$ MPa, $\nu = 0.5$ we estimated the mean radius of curvature $R_{\text{micro}} \approx 2.6$ mm. In Fig. 9, $\widetilde{\alpha}_A$ is shown as a function of $\widetilde{A}_0$ (green solid line), with superimposed the experimental data obtained for smooth spheres (black triangles) and microjunctions (raw data: gray crosses; averaged data: purple squares). The agreement between the model and the experimental results is very good over more than two orders of magnitude in $\widetilde{A}_0$ but cannot be assessed in the range $1 < \widetilde{A}_0 < 10$. Indeed JKR theory predicts, under force control, that the smallest stable contact spot is $\widetilde{A}_{\text{min,JKR}} = \pi(\frac{9\pi}{8})^{2/3} \simeq 7.3$.

Discrepancies may arise at too small contact areas as the decay law may not be strictly quadratic anymore, as indeed recent investigations seem to suggest [8,23]. We reconsidered the obtained area-force curves and fitted them using a power law function with form $A(Q) = A_0 - c_1 Q^n$, from which the best-fit exponent n has been obtained. Figure 10(a) shows the quantity $1 - A(Q)/A_0$ as a function of Q in a log-log plot. The red dots represent the points obtained using the elliptical model, while the black solid lines are the best-fitted power law functions obtained varying the normal force P over four orders of magnitude. One easily recognizes that the lighter the normal force the steeper gets the power law function, suggesting that a unique exponent is unlikely to best fit all the curves. In Fig. 10(b) n is reported as a function of the normal force P (solid curve). The shaded areas indicate the range of normal forces used in the experiments by Sahli *et al.* [15] and Mergel *et al.* [8]. Inspection of the graph reveals that for the

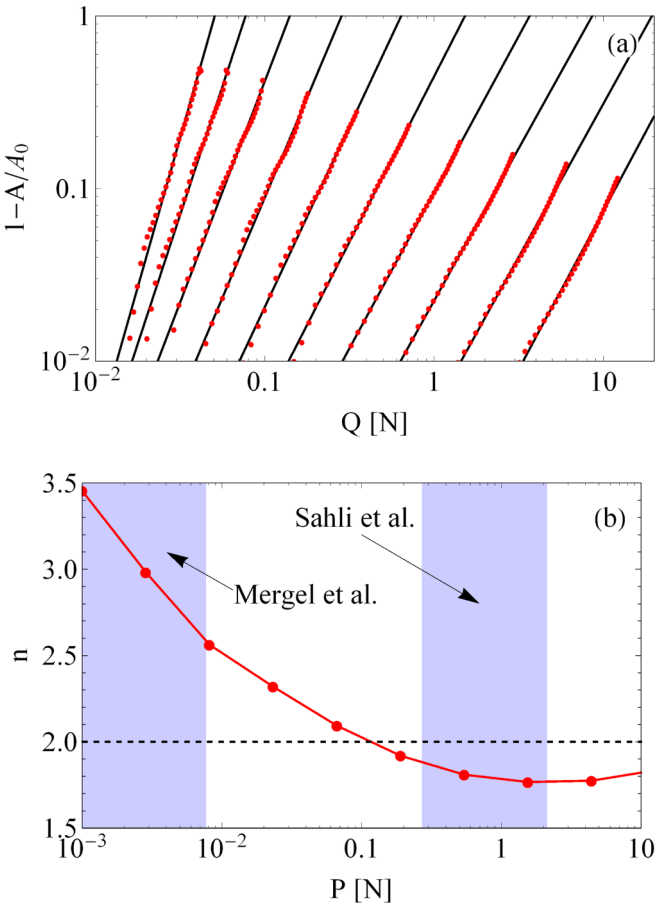

FIG. 10. (a) Best fit of the form $1 - A(Q)/A_0 \propto Q^n$ applied to the numerical data obtained by the proposed elliptical model for a range of normal forces ranging from 1 mN to 10 N, from left to right. Red dots represent the numerical data, while the solid black lines stand for the best-fitted power law. The exponent n is reported in panel (b) as a function of the normal force. Shaded areas indicate the regions where Sahli *et al.* [15] and Mergel *et al.* [8] data lie.

experiments in Ref. [15] normal forces are of the order of 1 N and the contact area decay in the model is well fitted by a quadratic power law ($n \approx 1.8$–1.9), while for lighter normal forces of the order of 10^{-3} to 10^{-2} N, as in Ref. [8], a larger exponent is found, $n \approx 3 \pm 0.5$.

VII. CONCLUSIONS

We have introduced a nonaxisymmetric model which successfully predicts the anisotropic shearing of the contact area under adhesive conditions due to tangential force. The model has been validated against several experimental data from Sahli *et al.* [15] and included in the companion Letter [25], and essentially an excellent agreement is found. The model is based on LEFM and has been inspired by the seminal work of JG [27], which has been extended to accomplish tangential loading of the contact area. Using our elliptical model we have made predictions of contact area evolution for nonaxisymmetric punches. The results show that the effect of differing principal radii of curvature strongly affects the evolution of the contact shape. This may be revealed to be a fundamental phenomenon in the development of contact patch anisotropy in rough contact under shear, where asperities are expected to be mildly elliptical [26]. We have also shown that in terms of overall variation of contact area a reduction of 10%–15% can be expected varying R_2/R_1 from 1 to 1/10. Deviations from this behavior may be expected due to the interactions between asperities, but this is out of the scope of the present paper.

ACKNOWLEDGMENTS

A.P. is thankful to the DFG (German Research Foundation) for funding the project PA 3303/1-1 and to Prof. Norbert Hoffmann for having supported his research studies. M.C. is supported by the Italian Ministry of Education, University and Research (MIUR) under the Departments of Excellence Grant No. L.232/2016. This work was supported by LABEX MANUTECH-SISE (ANR-10-LABX-0075) of the Université de Lyon, within the program Investissements d'Avenir (ANR-11-IDEX-0007) operated by the French National Research Agency (ANR). It received funding from the People Program (Marie Curie Actions) of the European Union's Seventh Framework Program (FP7/2007-2013) under Research Executive Agency Grant Agreement PCIG-GA-2011-303871. We are indebted to Institut Carnot Ingénierie@Lyon for support and funding.

A.P. and M.C. conceived the theoretical model and wrote the work. A.P. created the figures. J.S., R.S., and G.P. provided the experimental data. All the authors revised the work to its final form.

[1] A. I. Vakis, V. A. Yastrebov, J. Scheibert, L. Nicola, D. Dini, C. Minfray, A. Almqvist, M. Paggi, S. Lee, G. Limbert, J. F. Molinari, G. Anciaux, R. Aghababaei, S. Echeverri Restrepo, A. Papangelo, A. Cammarata, P. Nicolini, C. Putignano, G. Carbone, S. Stupkiewicz, J. Lengiewicz, G. Costagliola, F. Bosia, R. Guarino, N. M. Pugno, M. H. Müser, and M. Ciavarella, Modeling and simulation in tribology across scales: An overview, Tribol. Int. **125**, 169 (2018).

[2] K. Autumn, A. Dittmore, D. Santos, M. Spenko, and M. Cutkosky, Frictional adhesion: A new angle on gecko attachment, J. Exp. Biol. **209**, 3569 (2006).

[3] D. Labonte and W. Federle, Biomechanics of shear-sensitive adhesion in climbing animals: Peeling, pre-tension and sliding-induced changes in interface strength, J. R. Soc. Interface **13**, 20160373 (2016).

[4] N. Gravish, M. Wilkinson, and K. Autumn, Frictional and elastic energy in gecko adhesive detachment, J. R. Soc. Interface **5**, 339 (2008).

[5] K. L. Johnson, K. Kendall, and A. D. Roberts, Surface energy and the contact of elastic solids, Proc. R. Soc. London A **324**, 301 (1971).

[6] A. M. Homola, J. N. Israelachvili, P. M. McGuiggan, and M. L. Gee, Fundamental experimental studies in tribology: The transition from "interfacial" friction of undamaged molecularly smooth surfaces to "normal" friction with wear, Wear **136**, 65 (1990).

[7] H. Yoshizawa, Y. L. Chen, and J. N. Israelachvili, Fundamental mechanisms of interfacial friction. 1. Relation between adhesion and friction, J. Phys. Chem. **97**, 4128 (1993).
[8] J. C. Mergel, R. Sahli, J. Scheibert, and R. A. Sauer, Continuum contact models for coupled adhesion and friction, J. Adhes. (2018), doi:10.1080/00218464.2018.1479258.
[9] E. Rabinowicz, Influence of surface energy on friction and wear phenomena, J. Appl. Phys. **32**, 1440 (1961).
[10] E. Rabinowicz, Friction coefficients of noble metals over a range of loads, Wear **159**, 89 (1992).
[11] I. Svetlizky and J. Fineberg, Classical shear cracks drive the onset of dry frictional motion, Nature (London) **509**, 205 (2014).
[12] A. Papangelo and M. Ciavarella, Cattaneo–Mindlin plane problem with Griffith friction, Wear **342-343**, 398 (2015).
[13] A. Papangelo, M. Ciavarella, and J. R. Barber, Fracture mechanics implications for apparent static friction coefficient in contact problems involving slip-weakening laws, Proc. R. Soc. London A **471**, 20150271 (2015).
[14] A. R. Savkoor and G. A. D. Briggs, The effect of a tangential force on the contact of elastic solids in adhesion, Proc. R. Soc. London A **356**, 103 (1977).
[15] R. Sahli, G. Pallares, C. Ducottet, I. E. Ben Ali, S. Al Akhrass, M. Guibert, and J. Scheibert, Evolution of real contact area under shear and the value of static friction of soft materials, Proc. Natl. Acad. Sci. USA **115**, 471 (2018).
[16] J. W. Hutchinson, Mixed mode fracture mechanics of interfaces, Metal-Ceramic Interfaces **4**, 295 (1990).
[17] K. L. Johnson, Continuum mechanics modeling of adhesion and friction, Langmuir **12**, 4510 (1996).
[18] K. L. Johnson, Adhesion and friction between a smooth elastic spherical asperity and a plane surface, Proc. R. Soc. London A **453**, 163 (1997).
[19] J. F. Waters and P. R. Guduru, Mode-mixity-dependent adhesive contact of a sphere on a plane surface, Proc. R. Soc. London A **466**, 1303 (2010).
[20] V. L. Popov and A. V. Dimaki, Friction in an adhesive tangential contact in the Coulomb-Dugdale approximation, J. Adhes. **93**, 1131 (2017).
[21] A. Filippov, V. L. Popov, and S. N. Gorb, Shear induced adhesion: Contact mechanics of biological spatula-like attachment devices, J. Theor. Biol. **276**, 126 (2011).
[22] M. Ciavarella, Fracture mechanics simple calculations to explain small reduction of the real contact area under shear, Facta Universitatis, Series: Mech. Eng. **16**, 87 (2018).
[23] A. Papangelo and M. Ciavarella, On mixed-mode fracture mechanics models for contact area reduction under shear load in soft materials, J. Mech. Phys. Solids **124**, 159 (2019).
[24] J. W. Hutchinson and Z. Suo, Mixed mode cracking in layered materials, in *Advances in Applied Mechanics*, edited by J. W. Hutchinson and T. Y. Wu (Academic Press, Boston, 1992), Vol. 29, pp. 63–191.
[25] R. Sahli, G. Pallares, A. Papangelo, M. Ciavarella, C. Ducottet, N. Ponthus, and J. Scheibert, Shear-Induced Anisotropy in Rough Elastomer Contact, Phys. Rev. Lett. **122**, 214301 (2019).
[26] J. A. Greenwood, A simplified elliptic model of rough surface contact, Wear **261**, 191 (2006).
[27] K. L. Johnson and J. A. Greenwood, An approximate JKR theory for elliptical contacts, J. Phys. D **38**, 1042 (2005).
[28] L. A. Galin, *Contact Problems* (Springer, Netherlands, 2008).
[29] J. J. Kalker, On the rolling contact of two elastic bodies in the presence of dry friction, Ph.D. dissertation, Delft University of Technology, 1967.
[30] https://commons.wikimedia.org/wiki/File:Fracture_modes_v2.svg.
[31] D. Maugis, *Contact, Adhesion and Rupture of Elastic Solids* (Springer, New York, 2000).
[32] K. L. Johnson, *Contact Mechanics* (Cambridge University Press, Cambridge, 1985).